Examinations of the early degrees of freedom in ultrarelativistic nucleus-nucleus collisions

P. Moreau,[1] O. Linnyk,[2] W. Cassing,[2] and E. L. Bratkovskaya[1,3]
[1]*Frankfurt Institute for Advanced Studies, Johann Wolfgang Goethe Universität, Frankfurt am Main, Germany*
[2]*Institut für Theoretische Physik, Universität Gießen, Germany*
[3]*Institute for Theoretical Physics, Johann Wolfgang Goethe Universität, Frankfurt am Main, Germany*
(Received 9 December 2015; revised manuscript received 15 February 2016; published 26 April 2016)

The parton-hadron string dynamics (PHSD) transport model is used to study the impact of the choice of initial degrees of freedom on the final hadronic and electromagnetic observables in Au+Au collisions at $\sqrt{s_{NN}} =$ 200 GeV. We find that a nonperturbative system of massive gluons (scenario I) and a system dominated by quarks and antiquarks (scenario II) lead to different hadronic observables when imposing the same initial energy-momentum tensor $T_{\mu\nu}(x)$ just after the passage of the impinging nuclei. In case of the gluonic initial condition the formation of $s,\bar{s}$ pairs in the quark-gluon plasma (QGP) proceeds rather slowly, such that the antistrange quarks and accordingly the K^+ mesons do not achieve chemical equilibrium even in central Au+Au collisions at $\sqrt{s_{NN}} = 200$ GeV. Accordingly, the K^+ rapidity distribution is suppressed in the gluonic scenario, and is in conflict with the data from the BRAHMS Collaboration. The proton and antiproton rapidity distributions also disfavor scenario I. Furthermore, a clear suppression of direct photon and dilepton production is found for the pure gluonic initial conditions, which is not so clearly seen in the present photon and dilepton spectra from Au+Au collisions at $\sqrt{s_{NN}} = 200$ GeV due to a large contribution from other channels. It is argued that dilepton spectra in the invariant mass range $1.2 < M < 3$ GeV will provide a definitive answer once the background from correlated D-meson decays is subtracted experimentally.

DOI: 10.1103/PhysRevC.93.044916

I. INTRODUCTION

Ultrarelativistic nucleus-nucleus collisions allow us to study strongly interacting QCD matter under extreme conditions in heavy-ion experiments at the Relativistic Heavy-Ion Collider (RHIC) and the Large Hadron Collider (LHC). The experiments at the RHIC and the LHC have demonstrated that a stage of partonic matter is produced in these reactions which is in an approximate equilibrium for a couple of fm/c [1]. Due to the nonperturbative and nonequilibrium nature of relativistic nuclear reaction systems, their theoretical description is based on a variety of effective approaches ranging from hydrodynamic models with different initial conditions [2–11] to various kinetic approaches [12–22] or different types of hybrid models [23–30]. In the latter hybrid approaches the initial state models are followed by an ideal or viscous hydro phase which after hadronic freeze-out is followed up by a hadronic transport approach to take care of the final elastic and inelastic hadronic reactions.

In the ideal or viscous hydro calculations the initial conditions—at some finite starting time of the order of 0.3 to 0.5 fm/c—have to be evaluated either in terms of the (standard) Glauber model or other initial state scenarios, as in the IP-glasma model [31,32]. Furthermore, a color glass condensate (CGC) [33] is expected to lead to structures of smaller scale compared to the Glauber model, which incorporates fluctuations on the nucleon scale. However, in the hydrodynamic approaches only the equation of state enters, as well as transport coefficients such as the shear viscosity η that account for nonviscous phenomena, but nothing can be said about the nature of the microscopic effective degrees of freedom. This also holds for hybrid models as long as they employ a hydro phase. To our knowledge only microscopic transport approaches allow us to bridge the gap from p-p to p-A and A-A collisions in a unique way without introducing additional (and less controlled) parameters, and they are sensitive to the degrees of freedom in the system since their medium-dependent retarded propagators fix the entire time evolution.

The complexity of heavy-ion collisions is reduced essentially in the case of proton-nucleus collisions due to the expected dominance of the initial-state effects over final-state effects. Recently, we performed a microscopic transport study of p-Pb collisions at a nucleon-nucleon center-of-mass energy $\sqrt{s_{NN}} = 5.02$ TeV and compared parton-hadron string dynamics (PHSD) results to the ALICE measurement at the LHC of the charged-particle pseudorapidity distributions from Ref. [34] for pseudorapidity $|\eta| < 2$ for different multiplicity bins of charged particles N_{ch} [35]. However, these differential pseudorapidity densities did not allow for firm conclusions on the initial state configuration and the dynamical degrees of freedom since other approaches compared reasonably well, too: the saturation models employing coherence effects [36–38] or the two-component models combining perturbative QCD processes with soft interactions [39,40]. On the other side, a sizable difference in the mean transverse momentum of particles $\langle p_T \rangle$ versus the pseudorapidity η with opposite slopes in η on the projectile side is found within the CGC framework relative to hydrodynamical or transport calculations [35]. Furthermore, an application of the same approach to Pb+Pb collisions at the collision energy $\sqrt{s_{NN}} = 2.76$ TeV showed that the heavy system is not sensitive to the size of initial state fluctuations [41] when concentrating on hadronic spectra and collective flow coefficients $v_2(p_T)$, $v_3(p_T)$, and $v_4(p_t)$. This finding was later confirmed in a viscous hydro model in Ref. [42]. In these studies the electromagnetic observables were discarded since the degrees of freedom in the initial stage were kept unchanged.

In this work we explore the sensitivity of hadronic and electromagnetic observables to the explicit initial degrees of freedom under the constraint of an identical energy-momentum tensor $T_{\mu\nu}(x)$ in the nonequilibrium phase just after the passage of the two imping nuclei (5% central Au-Au collisions at $\sqrt{s_{NN}} = 200$ GeV). We address this question by investigating two alternative scenarios for the initial production of the quark-gluon plasma: Scenario I involves purely gluonic initial states as proposed more than two decades ago in Refs. [43–47] since at that time a first-order phase transition from hadronic to partonic matter had been expected. This scenario was recently brought forward again in Ref. [48] due to a possibly gluon dominated initial state. Scenario II describes the initial plasma as a pure ensemble of quark and antiquark degrees of freedom (without gluons).

After a brief review of the PHSD off-shell transport approach, we explain the implementation of initial gluonic degrees of freedom in Sec. II and show the actual dynamical evolution of the quark and gluon numbers as well as the quark and gluon interaction rates for both scenarios in the case of central Au+Au collisions at $\sqrt{s_{NN}} = 200$ GeV. The PHSD calculations for various hadronic spectra, collective flows, and electromagnetic observables are presented in Sec. III in comparison to available data. We summarize our findings in Sec. IV.

II. REVIEW OF PHSD AND ITS EXTENSION

The PHSD model is a covariant dynamical approach for strongly interacting systems formulated on the basis of Kadanoff-Baym equations [49] or off-shell transport equations in phase-space representation, respectively. In the Kadanoff-Baym theory the field quanta are described in terms of dressed propagators with complex self-energies. Whereas the real part of the selfenergies can be related to mean-field potentials (of Lorentz scalar, vector or tensor type), the imaginary parts provide information about the lifetime and/or reaction rates of timelike particles [50]. Once the proper (complex) self-energies of the degrees of freedom are known, the time evolution of the system is fully governed by off-shell transport equations (as described in Refs. [49,50]). This approach allows for a simple and transparent interpretation of lattice QCD results for thermodynamic quantities as well as correlators and leads to effective strongly interacting partonic quasiparticles with broad spectral functions. For a review of off-shell transport theory we refer the reader to Ref. [50]; model results and their comparison with experimental observables for heavy-ion collisions from the lower Super Proton Synchrotron (SPS) to Relativistic Heavy-Ion Collider (RHIC) energies can be found in Refs. [21,22,51–53] including electromagnetic probes such as e^+e^- or $\mu^+\mu^-$ pairs [54,55] or real photons [56].

In the beginning of relativistic heavy-ion collisions, color-neutral strings (described by the FRITIOF Lund model [57]) are produced in hard scatterings of nucleons from the impinging nuclei. These strings are dissolved into "prehadrons" with a formation time of 0.8 fm/c in their rest frame, except for the "leading hadrons," i.e., the fastest residues of the string ends, which can re-interact (practically instantly) with hadrons with reduced cross sections in line with quark counting rules. If, however, the local energy density is larger than the critical value for the phase transition, which is taken to be ~ 0.5 GeV/fm^3, the prehadrons melt into (colored) effective quarks and antiquarks as well as massive gluons in their self-generated repulsive mean-field as defined by the dynamical quasiparticle model (DQPM) [50]. In the DQPM the quarks, antiquarks, and gluons are dressed quasiparticles and have temperature-dependent effective masses and widths which have been fitted to the lattice thermal quantities such as energy density, pressure, and entropy density. Furthermore, the interaction rates from the DQPM—entering, e.g., in the electric conductivity or shear viscosity of the hot QGP—have been successfully confronted with results from lattice QCD (lQCD) [58,59]. The nonzero width of the quasiparticles implies the off-shellness of partons, which is taken into account in the scattering and propagation of partons in the QGP on the same footing (i.e., propagators and couplings).

The transition from partonic to hadronic degrees of freedom is described by covariant transition rates for the fusion of quark-antiquark pairs to mesonic resonances or three quarks (antiquarks) to baryonic states, i.e., by dynamical hadronization [21,22]. Note that due to the off-shell nature of both partons and hadrons, the hadronization process obeys all conservation laws (i.e., four-momentum conservation and flavor current conservation) in each event, the detailed balance relations, and the increase in the total entropy S. In the hadronic phase PHSD is equivalent to the hadron string dynamics (HSD) model [18].

A. Extensions to gluonic initial states

To modify the PHSD model to gluonic initial states (scenario I) under the constraint of keeping the energy-momentum tensor $T_{\mu\nu}(x)$ unmodified with respect to the default PHSD approach, we exchange in the PHSD dissolution routine the massive quark and antiquark degrees of freedom by massive gluons alone, which are generated by the fusion of flavor-neutral quark and antiquark pairs of closest distance in phase space. Since in PHSD the gluonic degrees are massive too, and have broad spectral functions (or imaginary parts of the retarded propagators), this gluonic fusion happens at practically the same time as the conventional dissolution in PHSD (above a critical local energy density of $\epsilon_c \approx 0.5$ GeV/fm^3 in line with the DQPM and lattice QCD). We note in passing that the conversion of quarks and antiquarks to massive gluons is similar to the dissolution in default PHSD; however, here the local ratio of quarks and antiquarks to gluons is fixed by the ratio from the DQPM at the same local energy density ϵ. Since the DQPM evaluates this ratio in thermal equilibrium, the gluons are substantially suppressed relative to quarks and antiquarks due to their larger masses, i.e., $M_g(\epsilon) \approx 3/2 M_q(\epsilon)$. The default PHSD model is thus much closer to scenario II. As in conventional PHSD, the gluonic degrees of freedom decay to quarks and antiquarks in time, in line with their decay width and vice versa ($g \leftrightarrow q + \bar{q}$), and in accordance with unquenched lattice QCD. In this way energy and momentum as well as flavor currents are conserved throughout the calculation [21,22]. The only difference is the "formation time" of the "particles" here,

which is shorter for the "gluons" due to their higher mass and is given by the inverse transverse mass $1/\sqrt{\mathbf{p}^2 + M_g^2}$ in their rest frame where M_g is the mass of the gluonic quasiparticle in the local cell. In order to introduce scenario II in PHSD, we immediately decay the formed (colored) gluons to (colored) quarks + antiquarks according to spectral functions from the DQPM. We mention that a partly related investigation has recently been performed in the on-shell transport model of the Catania group [60]. We stress, however, that the default initialization in PHSD includes quark and antiquark as well as gluonic degrees of freedom that are populated in each local cell according to the DQPM [50]. Furthermore, similar strategies have been incorporated in Ref. [61] for the transition from DQPM degrees of freedom to those from the NJL model at a similar initial stage.

B. Parton abundancies

In order to illustrate the procedure we show in Fig. 1 the time evolution of the gluon number (solid red line) as well as the total quark+antiquark number (divided by 2) (dashed blue line) and strange+antistrange quark number (divided by 2) (dot-dashed green line) as a function of time t for a central ($b = 2$ fm) Au+Au collision at $\sqrt{s_{NN}} = 200$ GeV in logarithmic representation. Initially, the partonic degrees of freedom in scenario I are entirely represented by gluons (from the melting strings) which in time produce quark-antiquark pairs by gluon splitting. Consequently, the strange-antistrange quark pairs appear with a delay. Since the early decrease of the gluon number is approximately exponential, we may attribute a transition time τ_g to this decay which amounts to $\tau_g \approx 6$–8 fm/c which is roughly in line with the Boltzmann approach to multiparton scatterings (BAMPS) calculations from Ref. [20]. On the other hand the PHSD calculations with the initial condition of only massive quarks and antiquarks—as generated by the dissolution of formed hadrons via string decay in scenario II—shows a different time evolution [cf. Fig. 1(b)]: here the time evolution exhibits an approximately exponential decrease of the quark+antiquark number, while the gluons are formed in the first 2–3 fm/c, however, remain suppressed throughout the time evolution since no chemical equilibration is achieved.

It is important to point out that scenario I is different from the "gluonic initial state" proposed in Ref. [48]. In our case we use the properties of the retarded propagators for partons as fixed by the DQPM in comparison with unquenched lattice QCD for 2+1 flavors, while in Ref. [48] a quenched gluonic system is addressed with undergoes a first-order phase transition at $T \approx 270$ MeV and does not couple dynamically to quarks and antiquarks. Consequently, the degrees of freedom in the model of Ref. [48] are color neutral massive glueballs for temperatures below about 270 MeV, whereas in our case we deal with colored massive gluons in interaction with massive quarks and antiquarks as inherent in full (unquenched) QCD.

In order to shed some light on the actual dynamics, we display the quark interaction rate dN_q/dt (a) and the gluon interaction rate dN_g/dt (b) for both scenarios in Fig. 2 for a central ($b = 2$ fm) Au+Au collision at $\sqrt{s_{NN}} = 200$ GeV. In line with the different initializations, the quark interaction rate is substantially suppressed in scenario I while the gluon interaction rate is suppressed in scenario II. Without explicit representation we mention that the hadronization rate is slightly larger in scenario II than in the gluonic scenario I. The actual timescales within the PHSD for the transition from gluonic to partonic matter are comparable to those from the BAMPS model [20].

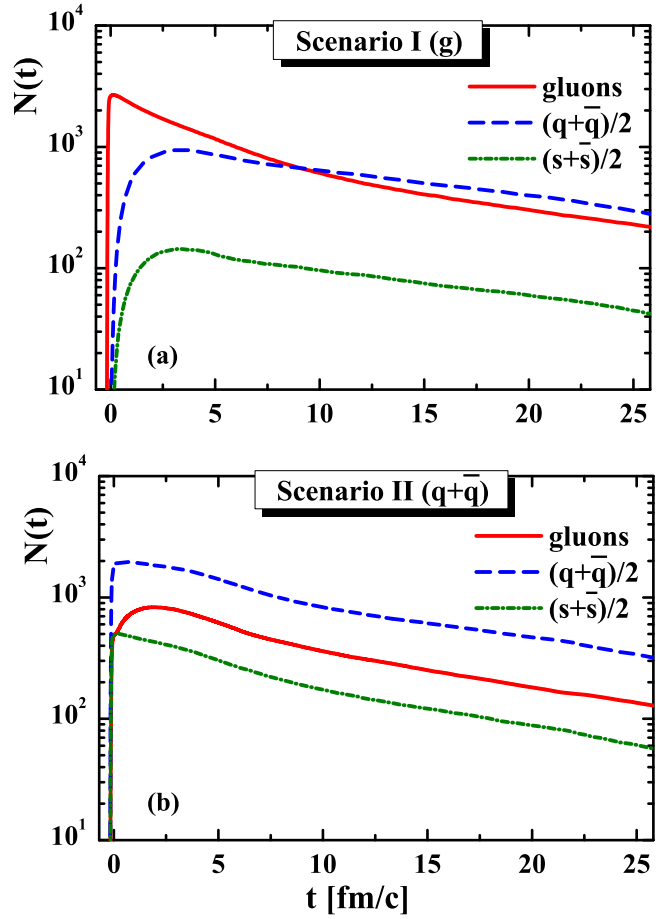

FIG. 1. (a) Time evolution of the gluon number (red solid line) as well as the total quark+antiquark number (divided by 2) (dashed blue line) and strange+antistrange quark number (divided by 2) (dot-dashed green line) as a function of time t for a central ($b = 2$ fm) Au+Au collision at $\sqrt{s_{NN}} = 200$ GeV in logarithmic representation for scenario I (gluonic initial conditions). (b) Same quantities as in (a) but for scenario II (fermionic initial conditions).

III. COMPARISON TO EXPERIMENTAL DATA

In this section we show the PHSD results for a variety of observables from 5% central Au+Au collisions at $\sqrt{s_{NN}} = 200$ GeV in comparison to experimental data by employing the different initial state scenarios I (gluons) and II (quarks and antiquarks). Note, however, that these different scenarios do not correspond to PHSD although the default version is closer to scenario II since in the DQPM the gluons are heavier than the quarks/antiquarks and suppressed relative to the quarks/antiquarks for fixed energy density in a given cell.

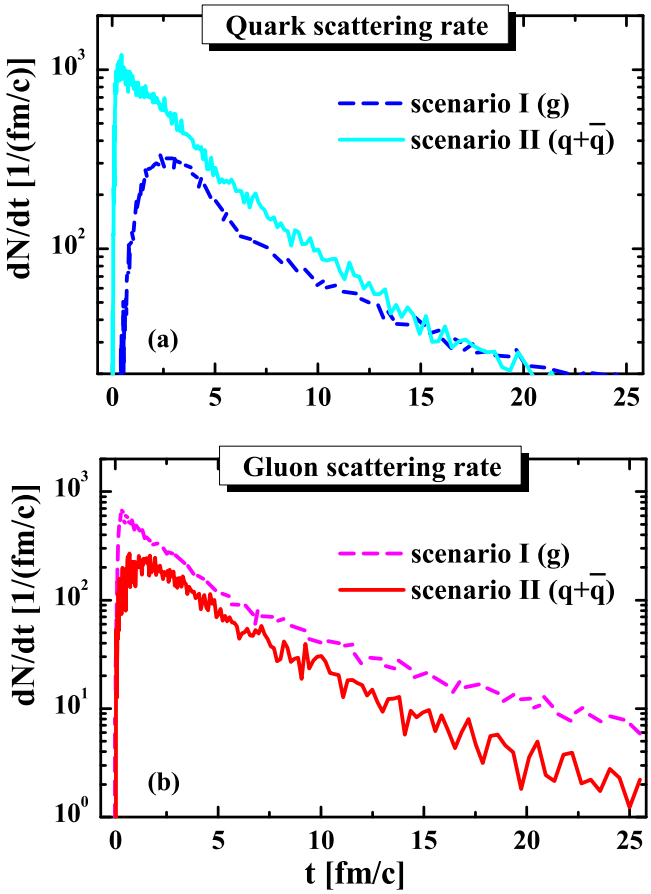

FIG. 2. (a) The quark interaction rate dN_q/dt from PHSD as a function of time t for a central ($b = 2$ fm) Au+Au collision at $\sqrt{s_{NN}} = 200$ GeV in scenario I (lower dark blue dashed line) and scenario II (light blue upper line). (b) Same quantities as in (a) but for the gluon interaction rate dN_g/dt (see legend).

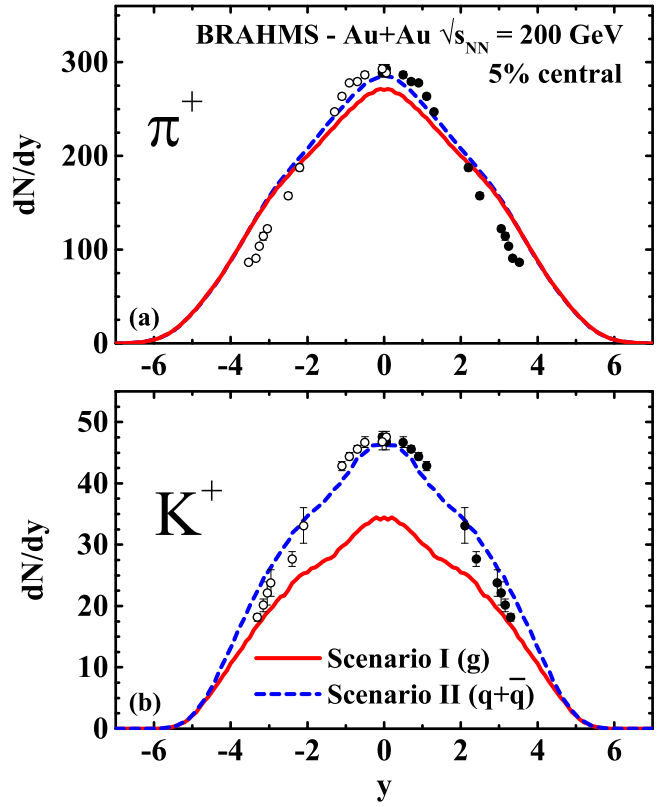

FIG. 3. Rapidity distributions for π^+ (a) and K^+ (b) mesons from PHSD for scenarios I and II in comparison to the results of the BRAHMS Collaboration [62] for 5% central Au+Au collisions at $\sqrt{s_{NN}} = 200$ GeV.

A. Hadronic observables

We start with 5% central Au+Au collisions at $\sqrt{s_{NN}} = 200$ GeV and compare in Fig. 3 the rapidity distributions for π^+ and K^+ mesons from scenarios I (red lines) and II (blue dashed lines) with the data from the BRAHMS Collaboration [62]. As expected from the previous section, there is only a slight difference in the pion rapidity distribution, however, the K^+ distribution is sizably underestimated in scenario I since the strange and antistrange quarks are out of chemical equilibrium and in scenario I not present at all in the beginning. We recall that the strangeness equilibration time for the partonic energies of interest in the PHSD is in the order of 20–30 fm/c [64], which is long compared to the duration of the partonic phase in central Au+Au collisions at the top RHIC energy. The slopes of the transverse momentum spectra (cf. Fig. 4) are quite similar for the two scenarios and slightly underestimate the data from Ref. [63].

The results for the proton and antiproton rapidity distributions are displayed in Fig. 5 for 5% central Au+Au collisions at $\sqrt{s_{NN}} = 200$ GeV in the two scenarios, and they demonstrate that scenario II with quarks and antiquarks in the initial state is clearly favored by the data from the BRAHMS [65] and PHENIX [63] collaborations.

The collective dynamics, however, might show a different picture since, e.g., the elliptic flow v_2 is driven by collisions as well as the repulsive scalar partonic potential as defined by the DQPM. The actual comparison of the PHSD results for scenarios I and II is displayed in Fig. 6 for the elliptic flow $v_2(p_T)$ of charged hadrons for minimum bias Au+Au collisions at $\sqrt{s_{NN}} = 200$ GeV. Unfortunately, there is almost no difference between the two scenarios, while both assumptions are compatible with the STAR data from Ref. [66].

B. Electromagnetic observables

We recall that in Ref. [67] the authors suggested investigating asymmetric nucleus-nucleus collisions in order to find out if in the very initial phase—during the passage time of the impinging nuclei—electric partonic charges are present, since the asymmetric electric field generated by the spectator protons would lead to different directed flows of particles and antiparticles (of opposite electric charge). In the case of symmetric nucleus-nucleus collisions, such an initial Coulomb boost from the spectator protons approximately cancels in the center of the partonic medium. In case of electromagnetic observables, we expect the yields and distributions of photons and dileptons to be quite sensitive to the initial degrees of freedom (being

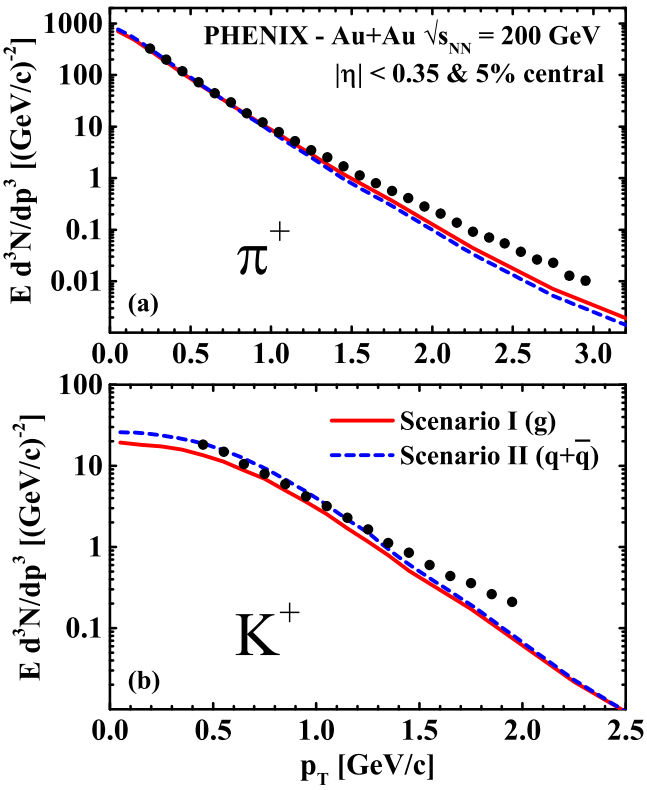

FIG. 4. Transverse momentum spectra for π^+ (a) and K^+ (b) mesons from PHSD for scenarios I and II in comparison to the results of the PHENIX Collaboration [63] for 5% central Au+Au collisions at $\sqrt{s_{NN}} = 200$ GeV.

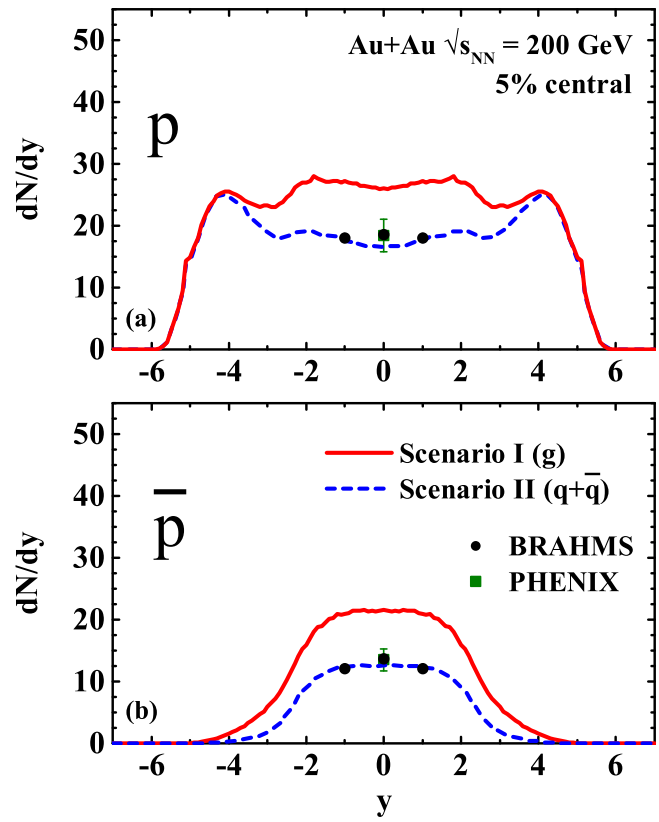

FIG. 5. The rapidity distribution of protons (a) and antiprotons (b) for 5% central Au+Au collisions at $\sqrt{s_{NN}} = 200$ GeV from scenarios I and II in comparison to the experimental data from the BRAHMS [65] and PHENIX collaborations [63] (the data as well as calculations are without including the feed–down from strange baryons).

charged or not). Especially the production of energetic photons by $q + \bar{q}$ annihilation should be substantially suppressed in scenario I [68,69] as compared to scenario II where quarks and antiquarks are present almost from the very beginning. Since also intermediate mass dileptons were found to be dominated by the $q + \bar{q}$ annihilation [54], this expectation should also hold for the virtual photons.

In order to quantify this expectation we have performed PHSD calculations for scenarios I and II, following up our previous studies in Refs. [54,56] where all the details of the calculations are presented. We recall that also the computation of the electromagnetic radiation from partons has been evaluated with the DQPM propagators such that no new parameter enters these calculations (cf. Ref. [70] for a recent review). In Fig. 7 we show the corresponding PHSD results for the two scenarios in comparison to the thermal photon data from PHENIX [71] for 0–20% centrality (a) and 20–40% centrality (b). The partonic photon contribution from q-$\bar{q}$ annihilation and gluon Compton scattering is displayed in terms of the green dashed lines for scenario II and the dash-dotted purple lines for scenario I. The solid red lines reflect the thermal photon spectrum when adding the hadronic channels—dominated by mm and mB bremsstrahlung—for scenario I while the dash-dotted blue line represents the same quantity for scenario II. We find that the partonic contribution is about an order of magnitude larger in scenario II than in the gluonic scenario I; however, when adding up all contributions

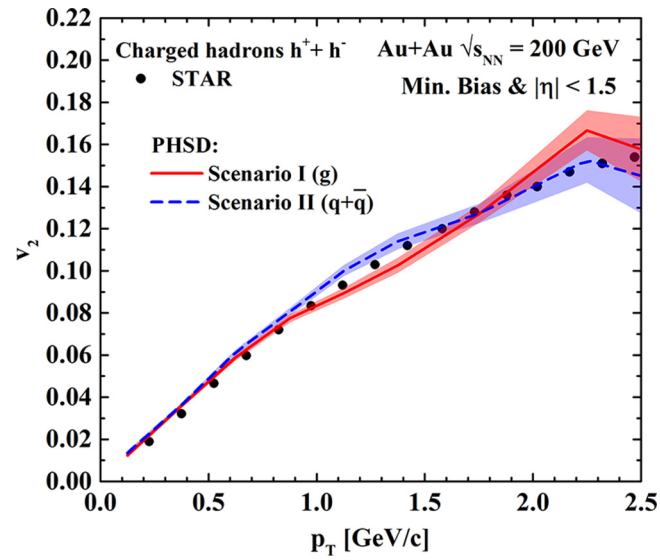

FIG. 6. The elliptic flow $v_2(p_T)$ of charged hadrons for minimum bias Au+Au collisions at $\sqrt{s_{NN}} = 200$ GeV from scenarios I and II in comparison to the experimental data from the STAR Collaboration [66].

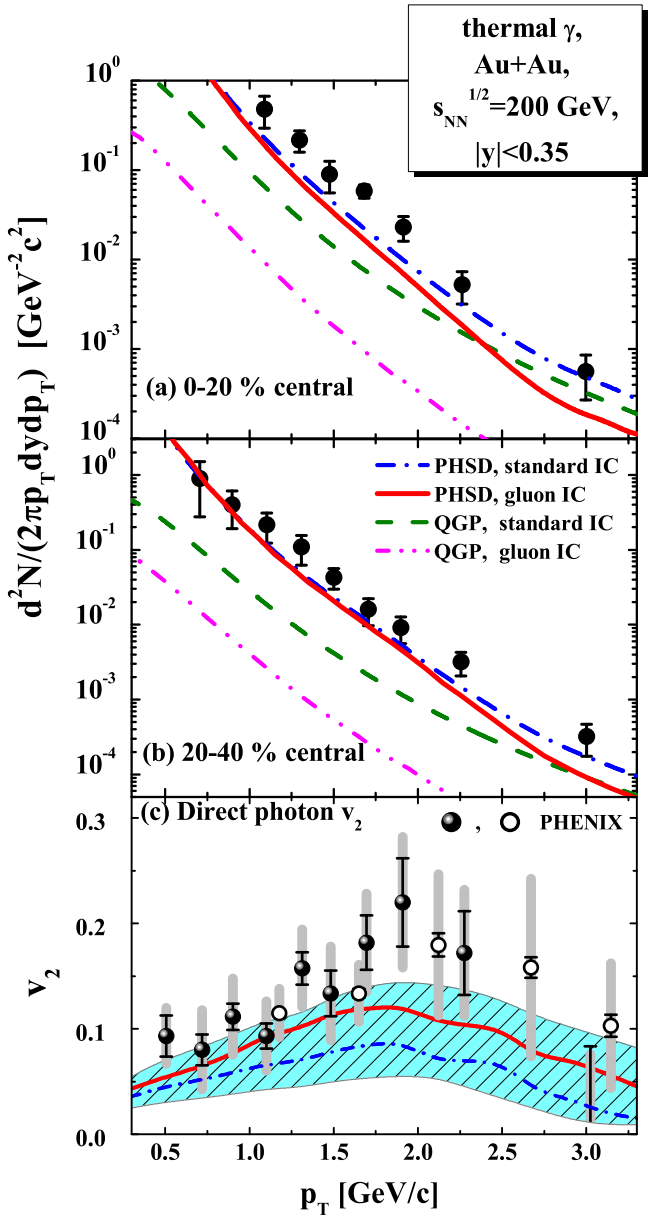

FIG. 7. The thermal photon yield from partonic channels versus transverse momentum p_T from PHSD (at midrapidity) in scenarios I (lower dash-dotted purple lines) and II (dashed green lines) for Au-Au reactions at $\sqrt{s_{NN}} = 200$ GeV for 0–20% centrality (a) and 20—40% centrality (b). The solid red lines reflect the thermal photon spectrum when adding the hadronic channels—dominated by mm and mB bremsstrahlung—for scenario I while the dash-dotted blue lines represent the same quantity for the scenario II. The data for the thermal photons are from the PHENIX Collaboration [71]. The panel (c) shows a comparison of the elliptic flow $v_2(p_T)$ for scenario I (solid red line) and scenario II (dashed blue line) with the PHENIX data. The hatched area displays the statistical uncertainty of the PHSD calculations.

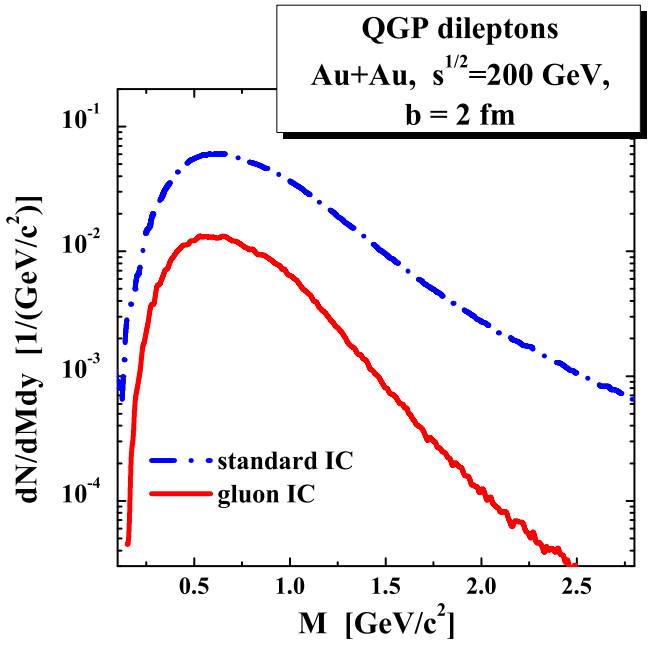

FIG. 8. Comparison of the QGP di-electron contribution as a function of the invariant mass M for scenario I (solid red line) and scenario II (dash-dotted blue line) for central Au+Au collisions at $\sqrt{s_{NN}} = 200$ GeV from the PHSD.

only a moderate depletion of the spectrum is visible for $p_T > 2$ GeV/c, which is below the PHENIX data at the largest transverse momenta. Note, however, that the thermal photon yield is slightly underestimated by the PHSD calculations for the most central collisions. Accordingly, the present photon data do not clearly differentiate between the two scenarios. In addition, panel (c) in Fig. 7 shows a comparison of the elliptic flow $v_2(p_T)$ for scenario I (solid red line) and scenario II (dashed blue line) with the PHENIX data. Here the hatched area displays the statistical uncertainty of the PHSD calculations. Nevertheless, there is a clear tendency for a larger photon v_2 in scenario I which is readily understood in terms of a reduced and delayed production of photons in the QGP phase where the photons are emitted from quark and antiquark channels that have achieved a finite v_2 due to the strong gluon-gluon interactions before. In contrast, the charged hadrons are only sensitive to the sum of gluonic and quark/antiquark interactions as well as hadronic channels, and show no sensitivity to the different scenarios in $v_2(p_T)$ as noted before (cf. Fig. 6).

We now turn to dileptons where the virtuality (invariant mass) of the lepton pair serves as an additional degree of freedom. In Fig. 8 we show a comparison of the QGP di-electron contribution as a function of the invariant mass for scenario I (solid red line) and scenario II (dash-dotted blue line). Since the dilepton yield at higher masses (>1 GeV) is dominated by q-$\bar{q}$ annihilation we find a large difference between the two scenarios which increases with the invariant mass M. Depending on the background yield and possible subtraction, especially the e^+e^- yield from $1.2 < M < 3$ GeV should qualify as a proper observable to distinguish the two scenarios.

In Fig. 9 we compare the mass spectra of e^+e^- pairs from Au+Au reactions at $\sqrt{s_{NN}} = 200$ GeV for 0–80% centrality from STAR [72] (a) and 0–92% from PHENIX [73] (b) to the PHSD results for the two scenarios. The thermal dilepton

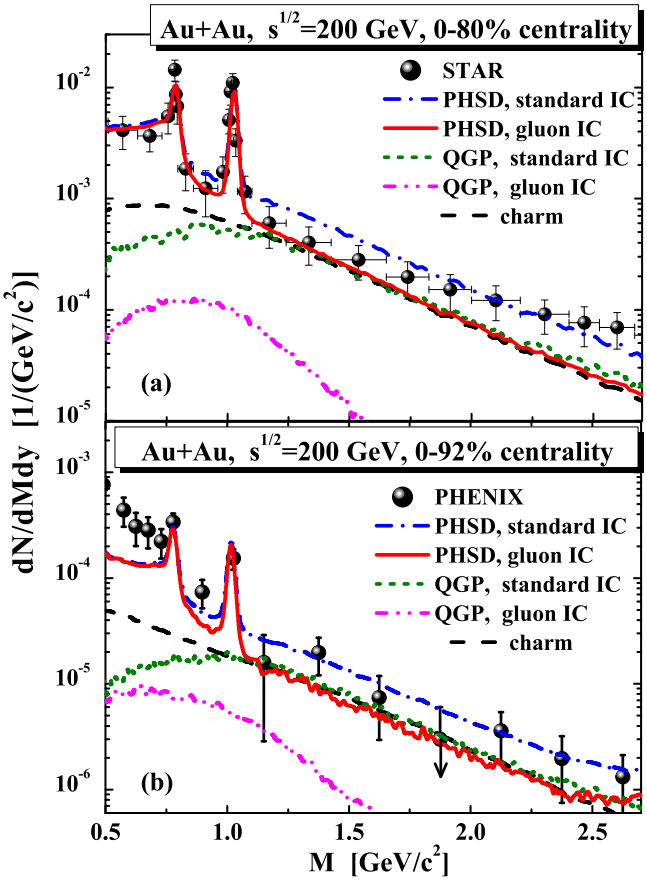

FIG. 9. The transverse mass spectra of e^+e^- pairs from Au+Au reactions at $\sqrt{s_{NN}} = 200$ GeV for 0–80% centrality (a) and 0–92% (b). The thermal dilepton yield from partonic channels is displayed for scenarios I (lower dash-dotted purple lines) and II (dashed green lines). The solid red lines reflect the total dilepton spectrum when adding the residual channels—dominated by correlated D-meson decays—for scenario I while the dash-dotted blue line represents the same quantity for scenario II. The dilepton data are from the STAR Collaboration [72] (a) and from the PHENIX Collaboration [73] (b).

yield from partonic channels is displayed for scenarios I (lower dash-dot purple lines) and II (dashed green lines) explicitly, and shows again very large differences depending on the initial degrees of freedom. Whereas in the case of scenario II the QGP contribution is roughly of the same size as the yield from correlated D-meson decays, the QGP yield from scenario I is practically not visible in the total spectra. The solid red lines in Fig. 9 reflect the total dilepton spectrum when adding the residual channels—dominated by correlated D-meson decays—for scenario I while the dash-dotted blue line represents the same quantity for scenario II. Whereas the present accuracy of the PHENIX data does not allow us to differentiate the different initial degrees of freedom, the STAR data show a better agreement with the PHSD calculations for scenario II. However, for a robust conclusion one needs to subtract the D-meson background as in, e.g., the NA60 data [74]. This gives a strong motivation for the STAR detector upgrade with a muon telescope [75].

IV. CONCLUSIONS

In this work the parton-hadron string dynamics (PHSD) approach has been employed in the top RHIC energy range for Au+Au collisions in order to explore the influence of the initial degrees of freedom on hadronic and electromagnetic observables. For this purpose we have considered two initial state scenarios: (I) with only massive gluons in the initial state (after the passage of the impinging nuclei) and (II) with only quarks and antiquarks while keeping the local energy-momentum tensor $T_{\mu\nu}(x)$ unchanged. We point out that the default PHSD approach does not correspond to these limiting scenarios, however, is closer to scenario II due to the thermal suppression of the gluons which are heavier than the quarks/antiquarks in the DQPM. In PHSD the equilibration between the gluonic and fermionic degrees of freedom proceeds dominantly via the channel $g \leftrightarrow q + \bar{q}$ with an equilibration time of order 6–8 fm/c. We find that the total partonic collision rates (adding up quarks/antiquarks and gluons) as well as the hadronization rate are not so different in the two scenarios. However, the formation of $s,\bar{s}$ pairs in the gluon dominated QGP (scenario I) proceeds rather slowly [64] such that the antistrange quarks and accordingly the K^+ mesons do not achieve chemical equilibrium even in central Au+Au collisions at the top RHIC energy. Accordingly, the K^+ rapidity distribution is suppressed in scenario I, in conflict with the data from BRAHMS.

Some comments on these results are in order: In scenario I the gluon decay to quark-antiquark pairs happens in accord with the gluon spectral function in PHSD that has a typical width of 100 to 150 MeV, which implies that the decay rate is rather "slow" (on timescales of 1.5 to 2 fm/c). In the case of gluon decay the ratio of strange to light quarks depends on the final phase space and thus on the quark masses. For the initial times this leads to a ratio of strange to light quarks of about 1/3; however, the quarks appear with a delay time of 1.5–2 fm/c relative to the gluons [cf. Fig. 1(a)], which is large compared to the average formation time of partons of 0.2–0.3 fm/c in scenario II. We recall that the concept of string melting in the QGP also implies a ratio of strange to light quarks of $\sim$1/3 [76]. One might claim that these widths might be substantially underestimated in the DQPM (or PHSD), but for substantially larger widths the ratio of the shear viscosity over entropy density η/s or the electric conductivity σ_e would drop by the same factors and no longer be in accord with results from lattice QCD (cf. the review [70]).

The rapidity distributions for protons and antiprotons are overestimated in the gluonic scenario I, while good agreement is achieved within scenario II in comparison to the data from the BRAHMS and STAR collaborations. The differential elliptic flow of charged particles (cf. Fig. 6) is not sensitive to the initial degrees of freedom; however, a drastic difference is seen in the photon and dilepton production from partonic sources since the initial gluonic degrees of freedom carry no electric charge. The actual comparison to the data from the PHENIX and STAR collaborations (cf. Figs. 7 and 9) slightly favor scenario II, i.e., the early presence of quarks and antiquarks; however, a robust conclusion (from the photon

data) will require more accurate measurements for transverse momenta of 2–3 GeV/c as well as a subtraction of the background from correlated D-meson decays in the case of dileptons.

ACKNOWLEDGMENTS

The authors are thankful to H. Stöcker for suggesting this study and for his continuous interest. Furthermore, they would like to thank M. Gorenstein and B. Kämpfer for valuable discussions and constructive proposals. Last but not least the authors acknowledge continuous discussions with J. Aichelin, H. Berrehrah, R.Marty, A. Palmese, E. Seifert and T. Steinert. This work in part was supported by the LOEWE center HIC for FAIR as well as by BMBF. P.M. acknowledges the financial support from the graduate school HGS-HIRe for FAIR. The computational resources were provided by the LOEWE-CSC.

[1] *Proceedings of Quark Matter–2014*, special issue of Nucl. Phys. A **931**, 1 (2014).
[2] P. Huovinen *et al.*, Phys. Lett. B **503**, 58 (2001).
[3] P. F. Kolb, P. Huovinen, U. Heinz, and H. Heiselberg, Phys. Lett. B **500**, 232 (2001).
[4] D. Teaney, J. Lauret, and E. V. Shuryak, Phys. Rev. Lett. **86**, 4783 (2001).
[5] T. Hirano and K. Tsuda, Phys. Rev. C **66**, 054905 (2002).
[6] P. F. Kolb and R. Rapp, Phys. Rev. C **67**, 044903 (2003).
[7] P. Huovinen, in *Quark-Gluon Plasma*, 3rd ed., edited by R. C. Hwa and X.-N. Wang (World Scientific, Singapore, 2004); P. F. Kolb and U. W. Heinz, *ibid.*
[8] P. Romatschke and U. Romatschke, Phys. Rev. Lett. **99**, 172301 (2007).
[9] H. Song and U. W. Heinz, Phys. Rev. C **77**, 064901 (2008).
[10] M. Luzum and P. Romatschke, Phys. Rev. C **78**, 034915 (2008).
[11] B. Schenke, S. Jeon, and C. Gale, Phys. Rev. C **82**, 014903 (2010).
[12] K. Geiger and B. Müller, Nucl. Phys. B **369**, 600 (1992).
[13] D. Molnar and M. Gyulassy, Phys. Rev. C **62**, 054907 (2000).
[14] S. Bass, B. Müller, and D. Srivastava, Phys. Lett. B **551**, 277 (2003).
[15] I. C. Arsene, L. V. Bravina, W. Cassing, Yu. B. Ivanov, A. Larionov, J. Randrup, V. N. Russkikh, V. D. Toneev, G. Zeeb, and D. Zschiesche, Phys. Rev. C **75**, 034902 (2007).
[16] S. Plumari, A. Puglisi, F. Scardina, and V. Greco, Phys. Rev. C **86**, 054902 (2012).
[17] S. A. Bass *et al.*, Prog. Part. Nucl. Phys. **41**, 255 (1998).
[18] W. Cassing and E. L. Bratkovskaya, Phys. Rep. **308**, 65 (1999).
[19] Z. W. Lin, C. M. Ko, B. A. Li, B. Zhang, and S. Pal, Phys. Rev. C **72**, 064901 (2005).
[20] Z. Xu and C. Greiner, Phys. Rev. C **71**, 064901 (2005); **76**, 024911 (2007); **81**, 054901 (2010).
[21] W. Cassing and E. L. Bratkovskaya, Nucl. Phys. A **831**, 215 (2009).
[22] E. L. Bratkovskaya, W. Cassing, V. P. Konchakovski, and O. Linnyk, Nucl. Phys. A **856**, 162 (2011).
[23] C. Nonaka and S. A. Bass, Phys. Rev. C **75**, 014902 (2007).
[24] H. Petersen and M. Bleicher, Phys. Rev. C **81**, 044906 (2010).
[25] G.-Y. Qin, H. Petersen, S. A. Bass, and B. Müller, Phys. Rev. C **82**, 064903 (2010).
[26] H. Song, S. A. Bass, and U. Heinz, Phys. Rev. C **83**, 024912 (2011).
[27] H. Petersen, C. Coleman-Smith, S. A. Bass, and R. Wolpert, J. Phys. G: Nucl. Part. Phys. **38**, 045102 (2011).
[28] H. Petersen, V. Bhattacharya, S. A. Bass, and C. Greiner, Phys. Rev. C **84**, 054908 (2011).
[29] H. Petersen, R. la Placa, and S. A. Bass, J. Phys. G **39**, 055102 (2012).
[30] H. Song, S. A. Bass, U. Heinz, T. Hirano, and C. S. Shen, Phys. Rev. Lett. **106**, 192301 (2011); **109**, 139904(E) (2012).
[31] B. Schenke, P. Tribedy, and R. Venugopalan, Phys. Rev. C **86**, 034908 (2012).
[32] C. Gale, S. Jeon, B. Schenke, P. Tribedy, and R. Venugopalan, Phys. Rev. Lett. **110**, 012302 (2013).
[33] F. Gelis, E. Iancu, J. Jalilian-Marian, and R. Venugopalan, Annu. Rev. Nucl. Part. Sci. **60**, 463 (2010); E. Iancu and R. Venugopalan, in *Quark-Gluon Plasma*, edited by R. Hwa and X. N. Wang (World Scientific, Singapore, 2003); H. Weigert, Prog. Part. Nucl. Phys. **55**, 461 (2005).
[34] B. Abelev *et al.* (ALICE Collaboration), Phys. Rev. Lett. **110**, 032301 (2013).
[35] V. P. Konchakovski, W. Cassing, and V. D. Toneev, J. Phys. G **41**, 105004 (2014).
[36] A. Dumitru, D. E. Kharzeev, E. M. Levin, and Y. Nara, Phys. Rev. C **85**, 044920 (2012).
[37] P. Tribedy and R. Venugopalan, Phys. Lett. B **710**, 125 (2012); **718**, 1154 (2013).
[38] J. L. Albacete, A. Dumitru, H. Fujii, and Y. Nara, Nucl. Phys. A **897**, 1 (2013).
[39] G. G. Barnafoldi, J. Barrette, M. Gyulassy, P. Levai, and V. Topor Pop, Phys. Rev. C **85**, 024903 (2012).
[40] R. Xu, W.-T. Deng, and X.-N. Wang, Phys. Rev. C **86**, 051901 (2012).
[41] V. P. Konchakovski, W. Cassing, and V. D. Toneev, J. Phys. G **42**, 055106 (2015).
[42] J. Noronha-Hostler, J. Noronha, and M. Gyulassy, Phys. Rev. C **93**, 024909 (2016).
[43] J. Alam, S. Raha, and B. Sinha, Phys. Rev. Lett. **73**, 1895 (1994).
[44] B. Kämpfer and O. P. Pavlenko, Z. Phys. C **62**, 491 (1994).
[45] T. S. Biro, E. van Doorn, B. Müller, M. H. Thoma, and X.-N. Wang, Phys. Rev. C **48**, 1275 (1993).
[46] M. Strickland, Phys. Lett. B **331**, 245 (1994).
[47] L. McLerran and R. Venugopalan, Phys. Rev. D **49**, 2233 (1994).
[48] H. Stöcker *et al.*, J. Phys. G **43**, 015105 (2016).
[49] S. Juchem, W. Cassing, and C. Greiner, Phys. Rev. D **69**, 025006 (2004); Nucl. Phys. A **743**, 92 (2004).
[50] W. Cassing, Eur. Phys. J. Spec. Top. **168**, 3 (2009); Nucl. Phys. A **795**, 70 (2007).
[51] V. D. Toneev, V. Voronyuk, E. L. Bratkovskaya, W. Cassing, V. P. Konchakovski, and S. A. Voloshin, Phys. Rev. C **85**, 034910 (2012).

[52] V. P. Konchakovski, E. L. Bratkovskaya, W. Cassing, V. D. Toneev, and V. Voronyuk, Phys. Rev. C **85**, 011902 (2012).
[53] V. P. Konchakovski, E. L. Bratkovskaya, W. Cassing, V. D. Toneev, S. A. Voloshin, and V. Voronyuk, Phys. Rev. C **85**, 044922 (2012).
[54] O. Linnyk, W. Cassing, J. Manninen, E. L. Bratkovskaya, and C. M. Ko, Phys. Rev. C **85**, 024910 (2012); O. Linnyk, E. L. Bratkovskaya, V. Ozvenchuk, W. Cassing, and C. M. Ko, *ibid.* **84**, 054917 (2011).
[55] O. Linnyk, W. Cassing, J. Manninen, E. L. Bratkovskaya, P. B. Gossiaux, J. Aichelin, T. Song, and C. M. Ko, Phys. Rev. C **87**, 014905 (2013).
[56] O. Linnyk, V. Konchakovski, T. Steinert, W. Cassing, and E. L. Bratkovskaya, Phys. Rev. C **92**, 054914 (2015); O. Linnyk, W. Cassing, and E. L. Bratkovskaya, *ibid.* **89**, 034908 (2014); O. Linnyk, V. P. Konchakovski, W. Cassing, and E. L. Bratkovskaya, *ibid.* **88**, 034904 (2013).
[57] B. Andersson, G. Gustafson, and H. Pi, Z. Phys. C **57**, 485 (1993).
[58] V. Ozvenchuk, O. Linnyk, M. I. Gorenstein, E. L. Bratkovskaya, and W. Cassing, Phys. Rev. C **87**, 064903 (2013).
[59] W. Cassing, O. Linnyk, T. Steinert, and V. Ozvenchuk, Phys. Rev. Lett. **110**, 182301 (2013); T. Steinert and W. Cassing, Phys. Rev. C **89**, 035203 (2014).
[60] F. Scardina, M. Colonna, S. Plumari, and V. Greco, Phys. Lett. B **724**, 296 (2013); M. Ruggieri, S. Plumari, F. Scardina, and V. Greco, Nucl. Phys. A **941**, 201 (2015).
[61] R. Marty, E. Bratkovskaya, W. Cassing, and J. Aichelin, Phys. Rev. C **92**, 015201 (2015).
[62] I. G. Bearden *et al.* (BRAHMS Collaboration), Phys. Rev. Lett. **94**, 162301 (2005).
[63] S. S. Adler *et al.* (PHENIX Collaboration), Phys. Rev. C **69**, 034909 (2004).
[64] V. Ozvenchuk, O. Linnyk, M. I. Gorenstein, E. L. Bratkovskaya, and W. Cassing, Phys. Rev. C **87**, 024901 (2013)
[65] I. Arsene *et al.* (BRAHMS Collaboration), Phys. Rev. C **72**, 014908 (2005).
[66] J. Adams *et al.* (STAR Collaboration), Phys. Rev. C **72**, 014904 (2005)].
[67] V. Voronyuk, V. D. Toneev, S. A. Voloshin, and W. Cassing, Phys. Rev. C **90**, 064903 (2014).
[68] B. Kämpfer, O. P. Pavlenko, A. Peshier, and G. Soff, Phys. Rev. C **52**, 2704 (1995).
[69] C. T. Traxler, H. Vija, and M. H. Thoma, Phys. Lett. B **346**, 329 (1995).
[70] O. Linnyk, E. L. Bratkovskaya, and W. Cassing, Prog. Part. Nucl. Phys. **87**, 50 (2016).
[71] A. Adare *et al.* (PHENIX Collaboration), Phys. Rev. Lett. **104**, 132301 (2010); Phys. Rev. C **91**, 064904 (2015)
[72] J. Zhao (STAR Collaboration), J. Phys. G **38**, 124134 (2011); L. Adamczyk *et al.* (STAR Collaboration), Phys. Rev. C **92**, 024912 (2015); Phys. Rev. Lett. **113**, 022301 (2014); **113**, 049903 (2014).
[73] A. Adare *et al.* (PHENIX Collaboration), Phys. Rev. C **81**, 034911 (2010); S. Afanasiev *et al.* (PHENIX Collaboration), arXiv:0706.3034; A. Toia (PHENIX Collaboration), Nucl. Phys. A **774**, 743 (2006); Eur. Phys. J. C **49**, 243 (2007)
[74] J. Seixas *et al.*, J. Phys. G **34**, S1023 (2007).
[75] L. Ruan *et al.*, J. Phys. G **36**, 095001 (2009).
[76] W. Cassing, A. Palmese, P. Moreau, and E. L. Bratkovskaya, Phys. Rev. C **93**, 014902 (2016).